Research Paper https://doi.org/10.7733/jnfcwt.2020.18.4.497

Excitation and Emission Properties of Adsorbed U(VI) on Amorphous Silica Surface

Euo Chang Jung*, Tae-Hyeong Kim, Hee-Kyung Kim, Hye-Ryun Cho, and Wansik Cha
Korea Atomic Energy Research Institute, 111 Daedeok-daero 989 beon-gil, Yuseong-gu, Daejeon, Republic of Korea

(Received October 19, 2020 / Revised November 3, 2020 / Approved November 8, 2020)

In the geochemical field, the chemical speciation of hexavalent uranium (U(VI)) has been widely investigated by performing measurements to determine its luminescence properties, namely the excitation, emission, and lifetime. Of these properties, the excitation has been relatively overlooked in most time-resolved laser fluorescence spectroscopy (TRLFS) studies. In this study, TRLFS and continuous-wave excitation–emission matrix spectroscopy are adopted to characterize the excitation properties of U(VI) surface species that interact with amorphous silica. The luminescence spectra of U(VI) measured from a silica suspension and silica sediment showed very similar spectral shapes with similar lifetime values. In contrast, the excitation spectra of U(VI) measured from these samples were significantly different. The results show that distinctive excitation maxima appeared at approximately 220 and 280 nm for the silica suspension and silica sediment, respectively.

Keywords: Time-resolved laser fluorescence spectroscopy (TRLFS), Excitation–emission matrix (EEM) spectroscopy, Adsorption, Hexavalent uranium, Amorphous silica

*Corresponding Author.
Euo Chang Jung, Korea Atomic Energy Research Institute, E-mail: ecjung@kaeri.re.kr, Tel: +82-42-868-4737

ORCID

Euo Chang Jung	http://orcid.org/0000-0002-6442-5791	Tae-Hyeong Kim	http://orcid.org/0000-0001-6483-5902
Hee-Kyung Kim	http://orcid.org/0000-0001-5840-7194	Hye-Ryun Cho	http://orcid.org/0000-0002-1293-6653
Wansik Cha	http://orcid.org/0000-0001-6153-1647		

1. Introduction

Studies on the interaction between uranium and silicon oxides, which are ubiquitous in the environment, are of interest in the research field of the final disposal of radioactive wastes. For example, the chemical form of uranium catalysts is typically a uranium-sorbed SiO_2 (silica), and the volume reduction of uranium-bearing spent catalysts is indispensable to reduce the disposal cost [1]. In addition, nuclear power plants generate radioactive wastes and they predominantly comprise uranium. The release of uranium from repository, entering the biosphere must be prevented for the long-term safety of radioactive waste disposal [2]. The sorption process of uranium onto amorphous silica and quartz surfaces has a significant effect on the migration properties of uranium. For these reasons, the physical and chemical interaction between uranium and silica has been an important research subject for decades [3].

Uranium exists in the form of highly luminescent hexavalent uranium (U(VI)) species under oxic conditions. The sorption characteristics of U(VI) were investigated at a molecular scale using several spectroscopic techniques, such as extended X-ray absorption fine structure spectroscopy [4-8], X-ray photoelectron spectroscopy [9, 10], and time-resolved laser fluorescence spectroscopy (TRLFS) [9-22]. Each spectroscopic technique has its advantages and disadvantages; however, TRLFS has received considerable attention due to its superior speciation sensitivity. The chemical speciation of U(VI) surface complexes at trace level concentrations is constantly progressing by determining the luminescence peaks and their lifetimes with a fixed excitation wavelength (λ_{ex}).

The excitation property of U(VI) species can also be used to distinguish one complex from another. Recently, the highly sensitive and specific excitation spectra of U(VI)-hydroxo complexes in aqueous solutions were extracted for the ultraviolet (UV) wavelength range of 180-370 nm [23]. These spectra explain the excitation wavelength-dependent luminescence intensities of dissolved U(VI) species reported by Moulin and coworkers [24]. They reported that the luminescence intensities for UO_2^{2+} and UO_2OH^+ in aqueous solutions are 10 and 40 times weaker, respectively, with λ_{ex} = 355 nm than with λ_{ex} = 266 nm. In contrast, the luminescence intensity for $(UO_2)_3(OH)_5^+$ is 5 times stronger with λ_{ex} = 355 nm than with λ_{ex} = 266 nm (with the same laser pulse energy and operating conditions). Although the excitation wavelength-dependent luminescence intensity of solid-state U(VI) compounds was reported by Wang et al. [25], the excitation property of the U(VI) surface species has rarely been studied.

In the present work, the excitation spectra of the U(VI) surface species adsorbed onto amorphous silica were investigated for two different silica samples at circumneutral pH. The excitation wavelength-dependent luminescence intensities were measured in the range of λ_{ex} = 200-500 nm using both TRLFS and continuous wave (CW) excitation-emission matrix (EEM) spectroscopy. Although the terms “luminescence” and “emission” can be used interchangeably, the “luminescence” and “emission” are used for TRLFS and EEM spectroscopy, respectively, to avoid confusion.

2. Material and Experimental

2.1 Material

A high-purity grade silica gel with a particle size of 40-63 μm (Sigma-Aldrich 227196) was used. The pore size of the silica gel reported by the manufacturer was approximately 6 nm (0.8 $cm^3 \cdot g^{-1}$ pore volume). Specific surface area was determined by the N_2 BET method to be approximately 477 $m^2 \cdot g^{-1}$. The silica gel was used to prepare a silica suspension and silica sediment with particle concentrations of 1 $g \cdot L^{-1}$ and 10 $g \cdot L^{-1}$, respectively. The adsorption reactions of uranium onto these silica samples were performed in 50 mL of a mixed solution (3.4 μM U(VI) and 0.1 M $NaClO_4$)

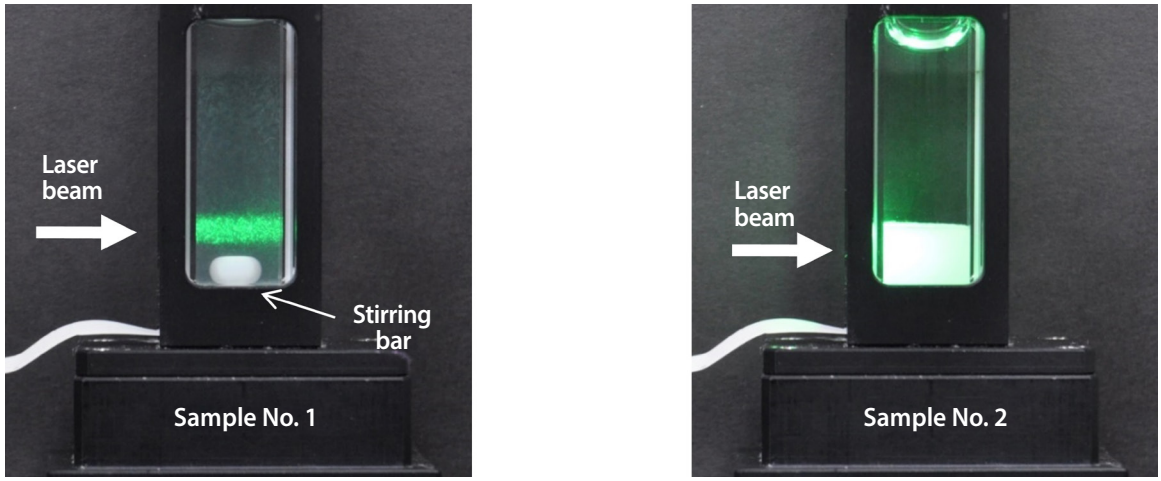

(a) (b)

Fig. 1. Photographs of the luminescence measured from sample No. 1 and sample No. 2. Stirring bar is placed at the bottom of the quartz cell in (a).

at a pH of 7.5. Samples were prepared by adding known amounts of silica to Millipore water, and reagents were added in the following order: 5.77 M $NaClO_4$, 1.5 mM UO_2^{2+} in 1.02 M $HClO_4$, which resulted in a pH of approximately 4.3. The desired pH conditions were achieved by adding known amounts of 0.1 M NaOH or $HClO_4$ determined from pre-titration processes. All sample preparations were carried out in an Ar-conditioned glove box with continuous stirring. Samples were further equilibrated in a rotary shaker for two or more days, after which the pH of the samples was measured using a glass combination electrode (Orion™, Ross Ultra).

The silica suspension prepared with particle concentrations of 1 $g \cdot L^{-1}$ was labeled to as "sample No. 1," and Fig. 1(a) shows the photograph of the luminescence measured from this sample. This sample (3 mL aliquot) was withdrawn from 50 mL of suspended solution and transferred to a quartz cell. The other solid-type silica sample prepared with particle concentrations of 10 $g \cdot L^{-1}$ was labeled "sample No. 2." The stock solution (50 mL of the mixed solution) was centrifuged for 30 min at 3,500 rpm, and the supernatant was decanted. The residual portion with the silica sediment was transferred to a quartz cell to prepare a silica sediment, as shown in Fig. 1(b). The laser beam path is clearly observed owing to the visible luminescence of the U(VI) surface species, as shown in Fig. 1(a). Conversely, only the luminescence generated from the sample surface was measured for sample No. 2, as shown in Fig. 1(b).

2.2 Spectroscopic instruments

Pulsed Nd: YAG lasers at 266 nm (Continuum, Minilite) and 355 nm (Continuum, Surelite) and optical parametric oscillators (OPOs) were used as the light sources. Two OPOs were operated at different wavelength ranges of 220-400 nm (Continuum, Horizon I) and 410-500 nm (OPOTEK, Vibrant B). All lasers were operated at a repetition rate of 10 Hz. The laser pulse energy was measured using an energy meter (Coherent, EPM 2000 with a J25LP-MB detector). The incident laser pulse energy was determined by measuring the laser beam passing through the empty quartz cell. The beam diameters were adjusted to approximately 2.5 mm using an iris diaphragm.

The luminescence perpendicular to the direction of propagation of the laser beam was guided using an optical fiber bundle (cross-section of 2 × 8 mm^2, 345 fibers).

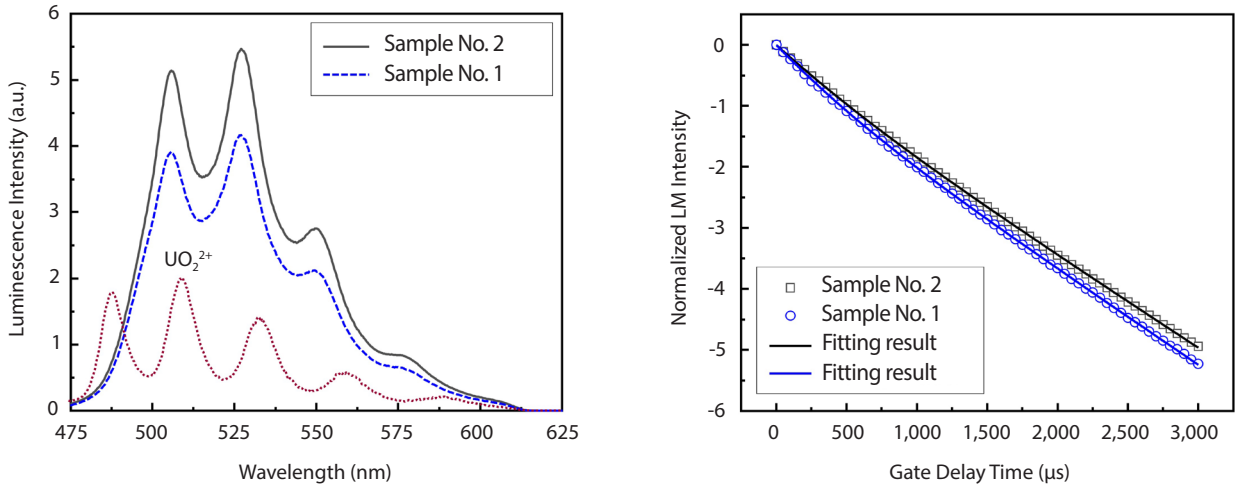

(a) (b)

Fig. 2. (a) Comparison of the luminescence spectra measured from samples No. 1 and No. 2 (pH 7.5) at λ_{ex} = 266 nm (the laser pulse energy of 0.1 mJ). The spectra were measured at t_d = 1 μs and t_w = 1,000 μs. Sample No. 2 was measured with approximately 9 times lower gain value of ICCD. The spectrum measured from UO_2^{2+} dissolved in aqueous solution at pH 1 is diaplayed as the dotted line for the comparison purpose.
(b) Luminescence (LM) lifetimes measured from the samples used as shown in Fig. 2(a). Symbols represent the normalized luminescence intensity in the natural logarithmic scale. The solid lines represent the fitting data calculated using Eq. (1) and the determined lifetimes were listed in Table 1.

The outlet of the optical fiber bundle was connected to a spectrograph (Andor, SR-303i). The time-resolved luminescence spectra were recorded by accumulating 100 laser pulses using two different gated intensified charge-coupled devices (ICCD, Andor, DH-720/18U-03 iStar 720D for λ_{ex} = 266, 355, and 410-500 nm, and DH320T-18U-93 for λ_{ex} = 220-400 nm) attached to the outlet ports of the spectrographs. All spectra were measured using a 1,000 μs gate width (t_w) and varying gate delay time (t_d).

CW EEM spectra were measured using a spectrofluorometer (Horiba Scientific, Aqualog) equipped with a 150 W ozone-free xenon arc lamp. Excitation spectra were recorded by scanning the excitation wavelength from 200 to 500 nm with a 2 nm step. Emission spectra were measured using a CCD in the wavelength range of 242-823 nm, with a resolution of 1.16 nm. The integration times were 5 and 0.5 s for samples No. 1 and No. 2, respectively. Since sample No. 2 generated a very strong emission intensity, a neutral density filter with approximately 9% transmission was inserted in front of the CCD for the EEM measurement of sample No. 2.

3. Results and Discussion

3.1 Time-resolved luminescence and lifetime properties

Time-resolved luminescence spectra and lifetimes measured with λ_{ex} = 266 nm at a laser pulse energy of 0.1 mJ are shown in Fig. 2. The t_d of the ICCD was set at 1 μs for all measurements. Although sample No. 2 was measured with approximately 9 times lower detection sensitivity with the low gain value of ICCD, the luminescence intensity of sample No. 2 was stronger than that of sample No. 1. The strong luminescence intensity of sample No. 2 is due to the concentrated silica particles in the silica sediment. The luminescence spectra of the two samples have similar spectral shapes with peak positions of 506, 527, 550, and 576 nm. This result implies that the microscopic environments affecting the luminescence properties of U(VI) are similar those affecting these two silica samples. For the comparison purpose, the luminescence spectrum measured from UO_2^{2+} dissolved in aqueous solution at pH 1 is also

Table 1. The determined lifetimes and relative contents of components 1 and 2.

Sample	Excitation wavelength (nm)	Component 1		Component 2		R^2
		α	τ_1 (μs)	1 - α	τ_2 (μs)	
No. 1	266	0.43	293	0.57	641	0.99995
	355	0.23	284	0.77	633	0.99955
No. 2	266	0.37	332	0.63	667	0.99998
	355	0.37	382	0.63	699	0.99922

illustrated as the dotted line in Fig. 2(a). The well-known luminescence peaks are located at approximately 488, 509, 533, 559, and 589 nm.

The luminescence lifetimes of U(VI) surface species measured from the samples shown in Fig. 2(a) are shown in Fig. 2(b). The luminescence intensities were measured using the kinetic mode of the ICCD. The t_d varied from 1-3,001 μs with a gate delay step of 50 μs. Consequently, the luminescence intensities of 61 spectra were used to determine the lifetime. The symbols shown in the data in Fig. 2(b) depict the normalized luminescence intensities in the natural logarithmic scale. Assuming that two U(VI) surface species formed the luminescence spectra, the lifetimes were fitted. The solid lines shown in Fig. 2(b) represent the result of fitting the data to the following double exponential decay equation using the Origin 9.5 program:

$$\ln\{I(t)\} = \ln\{a \times \exp(-\frac{t}{\tau_1}) + (1-a) \times \exp(-\frac{t}{\tau_2})\}, \quad (1)$$

where $I(t)$ is the normalized luminescence intensity integrated from 475-600 nm, and a and 1-a are the relative amounts of short- and long-lived components (called "component 1" and "component 2") with luminescence lifetimes of τ_1 and τ_2, respectively.

To obtain the best fitting results of relatively low uncertainty, we initially provided a measured lifetime of τ_2 as a 'known' parameter in the following subsequent processes. There were no significant changes in the peak wavelengths and spectral shapes of the normalized luminescence spectra measured in the range of t_d = 2,001-3,001 μs (data not shown). This result means that the τ_2 of component 2 can be determined by fitting the luminescence intensities in the natural logarithmic scale measured from t_d = 2,001-3,001 μs to the linear regressions with negligible interference of the luminescence intensity of component 1. Subsequently, τ_2 can be used as a known value to determine the τ_1 of component 1. The determined luminescence lifetimes and relative contents of components 1 and 2 are summarized in Table 1. The coefficients of determination (R squared) were higher than 0.999 for all fits.

Two different U(VI) surface species on SiO_2 were reported in most previous TRLFS studies [9, 13-16]. Components 1 and 2 are prominent in the acidic and circumneutral pH regions, respectively. Component 1 is a less tightly bound surface complex than component 2 [26]. It is speculated that the surface complexation of free U(VI) results in the formation of component 1 ($\equiv SiO_2UO_2$) [13]. A shift to a relatively long wavelength in the peak wavelengths of component 2 (data not shown) indicates the surface complexation of U(VI)-hydroxo species. Several species, such as $\equiv SiO_2(UO_2)OH^-$, $\equiv SiO_2(UO_2)_3(OH)_5^-$, and $\equiv SiO_2(UO_2)CO_3^-$, have been proposed for component 2 [9, 13]. However, these U(VI) surface species have not yet been fully identified. Moreover, a wide range of luminescence lifetime values has been reported for these U(VI) surface species prepared under comparable experimental conditions [9, 10, 13-16, 21]. Until now, the reason for these inconsistent lifetime values has not been clarified. The

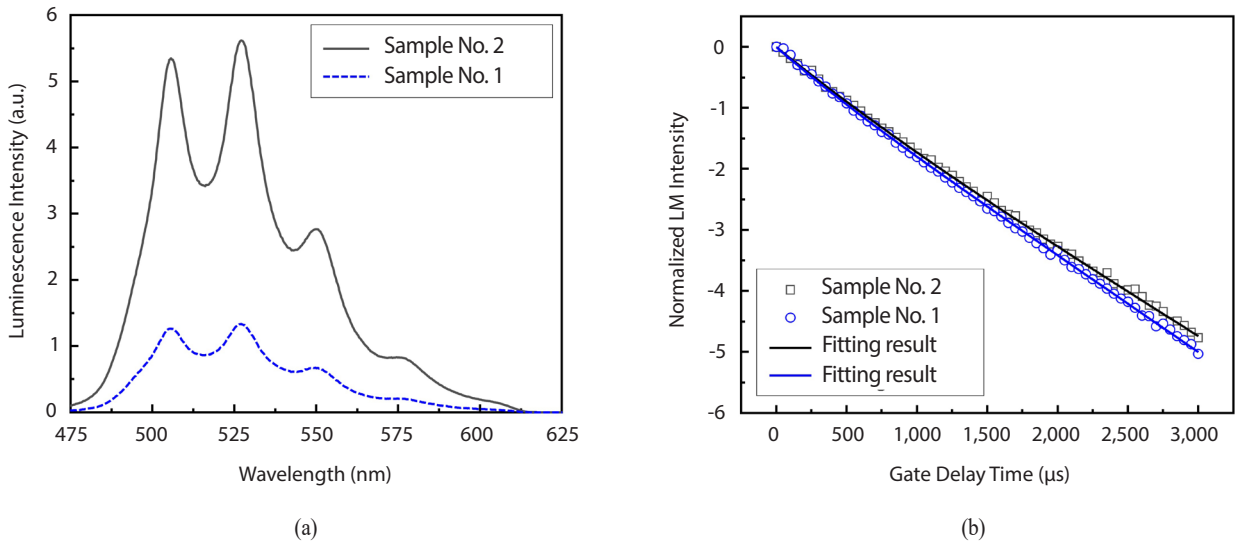

(a) (b)

Fig. 3. (a) Comparison of the luminescence spectra measured from samples No. 1 and No. 2 (pH 7.5) at λ_{ex} = 355 nm (the laser pulse energy of 2.0 mJ). The spectra were measured at t_d = 1 μs and t_w = 1,000 μs. Sample No.2 was measured with approximately 9 times lower gain value of ICCD. (b) Luminescence (LM) lifetimes measured from the samples used as shown in Fig. 3(a). Symbols represent the normalized luminescence intensity in the natural logarithmic scale. The solid lines represent the fitting data calculated using Eq. (1) and the determined lifetimes were also listed in Table 1.

Table 2. Relative luminescence intensities measured at different excitation wavelengths: The luminescence intensity of sample No. 1 measured at λ_{ex} = 355 nm was normalized to 1

Sample	Luminescence intensity	
	λ_{ex} = 266 nm	λ_{ex} = 355 nm
No. 1	65	1
No. 2	740	37

interpretation of the experimental data remains ambiguous, and it is beyond the scope of this study.

Time-resolved luminescence spectra and lifetimes measured with λ_{ex} = 355 nm at a laser pulse energy of 2.0 mJ are shown in Figs. 3(a) and (b), respectively. The experimental conditions of ICCD were the same as those used to measure the data displayed in Fig. 2. The luminescence lifetimes determined with λ_{ex} = 355 nm are also listed in Table 1. As mentioned in the previous paragraph, the measured lifetimes presented in Table 1 are much longer than those reported in the literature [9, 10, 13-16, 21]. However, this problem could not be solved in this study. Although the lifetimes determined with λ_{ex} = 355 nm are similar to the values determined with λ_{ex} = 266 nm (see Table 1), there are striking differences in the luminescence intensities in the data shown in Fig. 2(a) and that shown in Fig. 3(a). In comparison with the data in Fig. 2(a), the luminescence intensity of sample No. 2 shown in Fig. 3(a) is much stronger than that of sample No. 1. Since the linear dependence of the luminescence intensity on the laser pulse energy at λ_{ex} = 355 nm was observed (data not shown), the luminescence intensities shown in Fig. 3(a) were scaled down to the calculated luminescence intensities at a laser pulse energy of 0.1 mJ. Under the consideration of different laser pulse energies (0.1 mJ at 266 nm and 2.0 mJ at 355 nm) and different gain values of ICCD, the luminescence intensities shown in Fig. 2(a) and Fig 3(a) are compared in Table 2. The weakest luminescence intensity of sample No. 1 at λ_{ex} = 355 nm was normalized to 1; thus, the other values were relatively high. The luminescence intensity of sample No. 1 is approximately 65 times stronger with λ_{ex} = 266 nm than with λ_{ex} = 355 nm. The luminescence intensity of sample No. 2 is approximately 20 times stronger with

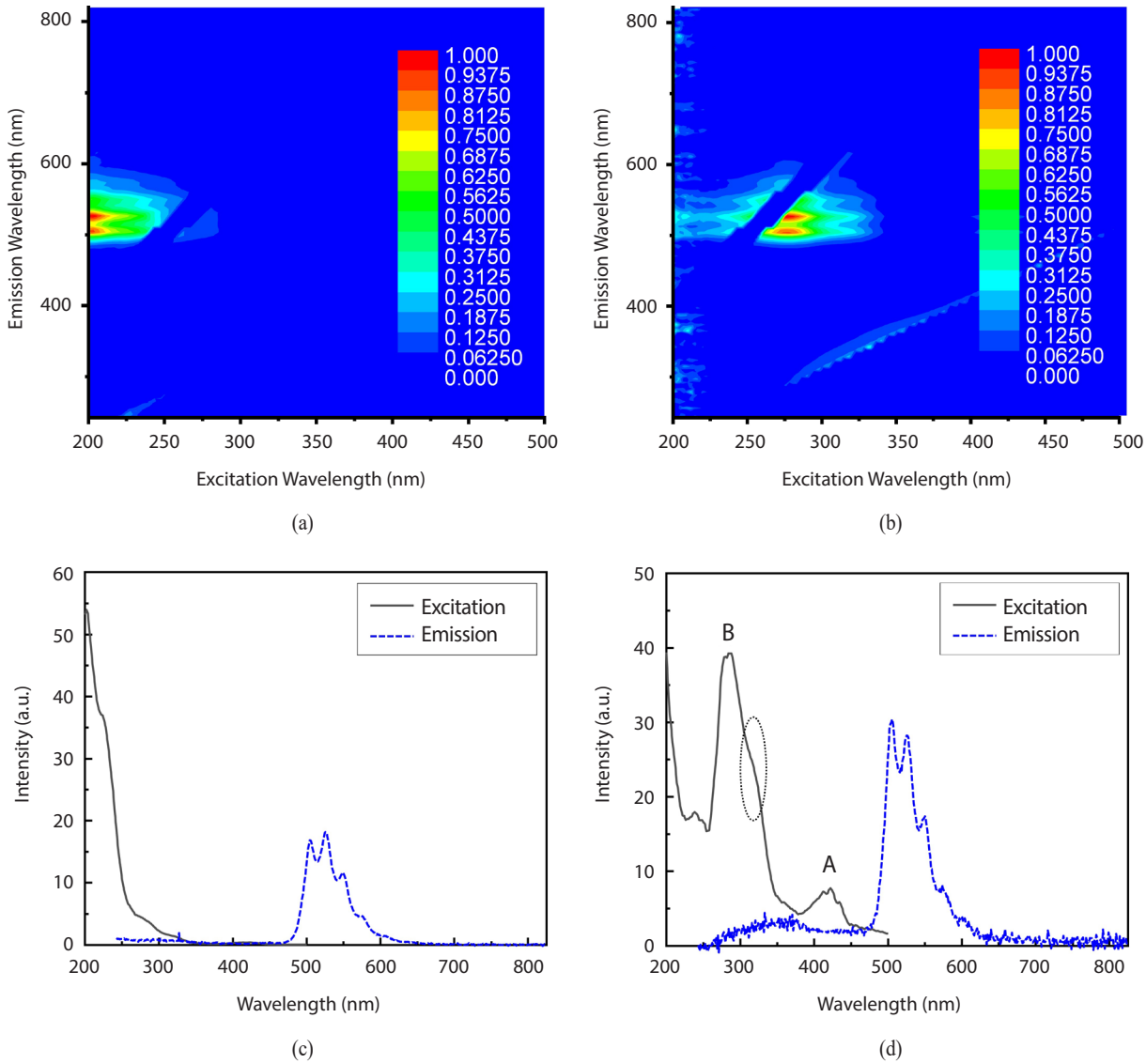

Fig. 4. EEM spectra measured from sample No. 1 (a) and sample No. 2 (b). The red color of these images represents stronger emission intensities than for other colors. The data (c) and (d) measured from samples No. 1 and No. 2, respectively, represent the overall excitation and emission spectra by summing the emission intensity values in the excitation mode. Band A and B appeared near 423 nm and 280 nm, respectively. The ellipse in (d) indicates the shoulder of band B near 320 nm.

λ_{ex} = 266 nm than with λ_{ex} = 355 nm. Contrarily, the luminescence intensities of sample No. 2 are approximately 11 and 37 times stronger with λ_{ex} = 266 nm and 355 nm, respectively, than those of sample No. 1. These results suggest different excitation properties for the silica suspension and the silica sediment.

3.2 Excitation properties

The absorption spectra of the U(VI) species dissolved in aqueous solutions were characterized by a very weak and broad absorption in the wavelength region of 370-520 nm [27]. The absorption cross section below

370 nm continued to increase to lower wavelengths [27-29]. The detailed absorption spectra of U(VI) surface species are less known than those of dissolved U(VI) species in aqueous solutions. For U(VI) surface species, the conventional UV/visible spectrophotometry was not appropriate to measure absorption spectrum in low concentrations (3.4 μM of U(VI) in the present study). In addition, the absorption spectrum of U(VI) surface species was interrupted by a severe light scattering of suspended silica particles. EEM spectroscopy is an effective method to verify the absorption properties of the adsorbed U(VI) species. However, the EEM spectra of U(VI) surface species are still limited.

Fig. 4 illustrates the representative EEM spectra of the U(VI) surface species, which visualize the complete emission profile at each excitation wavelength. The red color of these images represents stronger emission intensities than for other colors. Sample No. 1 shown in Fig. 4(a) exhibits emission intensities in the wavelength range of 475-625 nm in the excitation wavelength range of 200-275 nm. Strong emissions appeared when sample No. 1 was excited near the UV wavelength range of 200-225 nm. Sample No. 2 shown in Fig. 4(b) shows the emission intensities in the same wavelength range of 475-625 nm. However, strong emissions appeared at the excitation wavelength of 275-300 nm. The data in Figs. 4(c) and (d) measured from samples No. 1 and No. 2, respectively, represent the overall excitation and emission spectra by summing the emission intensity values in the excitation mode. The shapes of the emission spectra in the wavelength range of 475-625 nm are similar to the time-resolved luminescence spectra displayed in Fig. 2(a) and Fig. 3(a). These results mean that the shapes of emission spectra in both samples are essentially independent of the excitation wavelength. It is an interesting, unusual observation considering that the emission properties of actinides are generally closely correlated to the excitation property changes.

However, the dependence of emission intensities on the excitation wavelength is clearly observed as shown in Figs. 4(c) and (d). The excitation spectra measured from samples No. 1 and No. 2 show very strong intensity in the UV wavelength range below 350 nm. The abrupt increase in excitation intensity to the relatively short wavelength direction, as shown in Fig. 4(c), is consistent with the observation of the luminescence intensities with λ_{ex} = 266 nm, which are approximately 65 times stronger than those with λ_{ex} = 355 nm for sample No. 1 as presented in Table 2. In contrast, the excitation spectrum of sample No. 2 shows two bands denoted as A and B in Fig. 4(d). The peak maxima of bands A and B appeared at near 423 and 280 nm, respectively. Band A in the wavelength range of 380-450 nm shows the distinctively resolved vibrational fine structure of U(VI). This band, known as the fingerprint region, is assigned to the Laporte forbidden O-to-U ligand-to-metal charge transfer (LMCT) transition [30, 31]. The spectral shape of band A is very similar to the absorption spectrum of UO_2^{2+} in acidic pH [27, 28]. However, the position of the peaks shifts to longer wavelengths (412, 423, and 434 nm) compared with those of the absorption spectrum of UO_2^{2+} (403, 414, and 426 nm). Among three dominant U(VI)-hydroxo species; UO_2OH^+, $(UO_2)_2(OH)_2^{2+}$, and $(UO_2)_3(OH)_5^+$, the last two species were reported to exhibit absorption spectra, which are not adequately resolved [27]. Thus, we speculate that the obsereved excitation spectrum, which is adequately resolved, as shown in Fig. 4(d), was likely generated from $\equiv SiO_2(UO_2)OH^-$ surface species. Band B in the wavelength region of 250-375 nm is interpreted as the LMCT transitions from the equatorial ligands [30, 31]. It seems that band B, as shown in Fig. 4(d), has the shoulder designated as ellipse near 320 nm, which is also observed in the presence of aqueous uranyl complexes [32]. For sample No. 2, the relatively high concentration of the silanol group of silica sediments results in an increased number of silanol group binding to U(VI) in the equatorial plane than that of the silanol group of the silica suspension, which can account for the more prominent band B in the silica sediment. The band B observed only in sample No. 2 considerably explains the luminescence intensity of sample No. 2, which

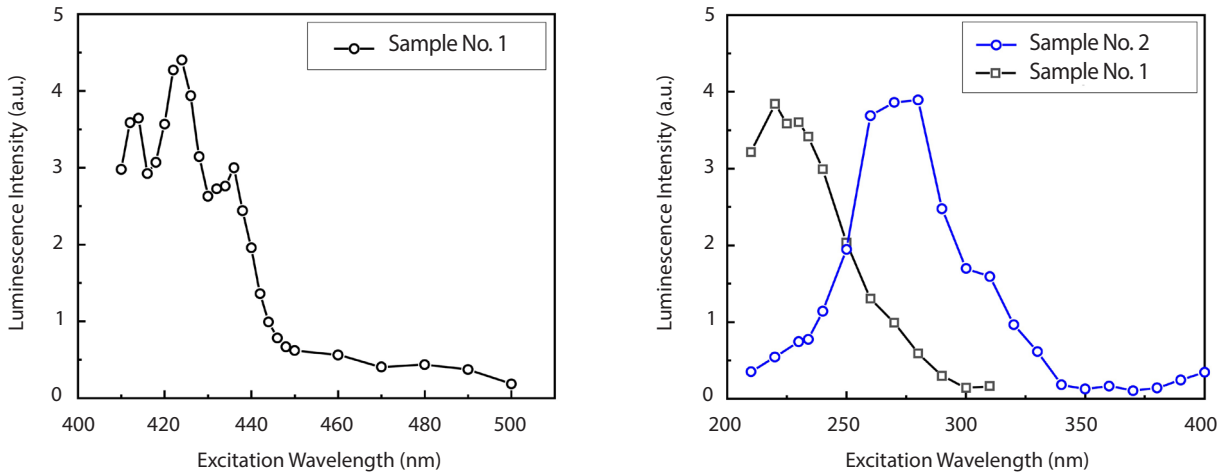

Fig. 5. (a) Excitation spectrum measured from sample No. 1 (pH 7.5). The luminescence intensities were obtained from the integration of the signal from 475-600 nm in the time-resolved luminescence spectrum measured at t_d = 1 μs. (b) Excitation spectra measured from samples No. 1 and No. 2 (pH 7.5). All data were measured under the same laser pulse energy of 0.2 mJ and operating conditions.

is approximately 37 times stronger than that of sample No. 1 with λ_{ex} = 355 nm, as shown in Table 2.

Finally, the excitation spectra measured using TRLFS were compared with the excitation spectra measured using EEM spectroscopy. The luminescence intensities displayed in Fig. 5 were obtained by integrating the signal from 475-600 nm in the time-resolved luminescence spectrum measured at t_d = 1 μs and t_w = 1000 μs. Fig. 5(a) shows the dependence of the time-resolved luminescence intensity on the excitation laser wavelength for sample No. 1. Although band A of sample No. 1 was hardly seen in the data presented in Fig. 4(c) due to the very weak O-to-U LMCT transition, the excitation spectrum shown in Fig. 5(a) is similar to that of band A measured from sample No. 2 using EEM spectroscopy, as shown in Fig. 4(d). The peak positions observed in Fig. 5(a) are the same as those observed in Fig. 4(d). Fig. 5(b) shows the excitation spectra measured using TRLFS in the excitation wavelength region of 210-400 nm for samples No. 1 and No. 2. The peak maxima appeared at approximately 220 nm and 280 nm for samples No. 1 and No. 2, respectively. The excitation spectrum of sample No. 1 seems to be similar to that of U(VI)-ligand complexes in acetonitrile medium, which shows a peak maximum of 246 nm [33]. These results confirm the different excitation properties between the silica suspension and the solid-type silica sediment. The reason for the different excitation pathways for these samples is not yet fully understood. In this study, we demonstrated that U(VI) surface species prepared at two different silica densities have distinctively different excitation properties, but their luminescence properties are not distinguishable. Further studies are required to identify the surface species. In particular, the coordination modes and numbers of bound silanol groups in each sample will be investigated in relation to the optical property changes.

4. Conclusion

Time-resolved luminescence spectra and lifetimes of U(VI) surface species were measured for the silica suspension and silica sediment. The luminescence spectra and lifetimes were similar at different excitation wavelengths of 266 nm and 355 nm, respectively. However, different

characteristics of luminescence intensities were obserevd at different excitation wavelengths. The former sample showed a very high luminescence yield at 266 nm than at 355 nm. In contrast, a relatively higher luminescence yield was observed at 355 nm for the latter sample than for the former sample. These characteristics are due to the different excitation properties between the two samples measured using both EEM spectroscopy and TRLFS. This result has not been previously reported, and further investigation on the fundamental properties of the U(VI) excitation pathway is required to understand the reason for this difference.

Acknowledgement

This study was supported by the Nuclear Research and Development program of the National Research Foundation of Korea (Grant code: 2017M2A8A-5014719).

REFERENCES

[1] K.W. Kim, M.J. Kim, M.K. Oh, J. Kim, H.H. Sung, R. I. Foster, and K.Y Lee, "Development of a treatment process and immobilization method for the volume reduction of uranium-bearing spent catalysts for final disposal", J. Nucl. Sci. Technol., 55(12), 1459-1472 (2018).

[2] J.I. Kim, "Significance of Actinide Chemistry for the Long-Term Safety of Waste Disposal", Nucl. Eng. Technol., 38(6), 459-482 (2006).

[3] H. Geckeis, J. Lützenkirchen, R. Polly, T. Rabung, and M. Schmidt, "Mineral-Water Interface Reactions of Actinides", Chem. Rev., 113(2), 1016-1062 (2013).

[4] T. Reich, H. Moll, M.A. Denecke, G. Geipel, G. Bernhard, H. Nitsche, P.G. Allen, J.J. Bucher, N. Kaltsoyannis, N.M. Edelstein, and D.K. Shuh, "Characterization of Hydrous Uranyl Silicate by EXAFS", Radiochim. Acta., 74, 219-223 (1996).

[5] T. Reich, H. Moll, T. Arnold, M.A. Denecke, C. Hennig, G. Geipel, G. Bernhard, H. Nitsche, P.G. Allen, J.J. Bucher, N.M. Edelstein, and D.K. Shuh, "An EXAFS Study of Uranium(VI) Sorption Onto Silica Gel and Ferrihydrite", J. Electron Spectrosc. Relat. Phenom., 96(1-3), 237-243 (1998).

[6] E.R. Sylwester, E.A. Hudson, and P.G. Allen, "The Structure of Uranium (VI) Sorption Complexes on Silica, Alumina, and Montmorillonite", Geochim. Cosmochim. Acta., 64(14), 2431-2438 (2000).

[7] M. Walter, T. Arnold, G. Geipel, A. Scheinost, and G. Bernhard, "An EXAFS and TRLFS Investigation on Uranium(VI) Sorption to Pristine and Leached Albite Surfaces", J. Colloid Interface Sci., 282(2), 293-305 (2005).

[8] M.S. Massey, J.S. Lezama Pacheco, J.M. Nelson, S. Fendorf, and K. Maher, "Uranium Incorporation into Amorphous Silica", Environ. Sci. Technol., 48(15), 8636-8644 (2014).

[9] A. Kowal Fouchard, R. Drot, E. Simoni, and J.J. Ehrhardt, "Use of Spectroscopic Techniques for Uranium(VI)/ Montmorillonite Interaction Modelling", Environ. Sci. Technol., 38(5), 1399-1407 (2004).

[10] R. Drot, J. Roques, and É. Simoni, "Molecular Approach of the Uranyl/Mineral Interfacial Phenomena", C. R. Chimie., 10(10-11), 1078-1091 (2007).

[11] J. Wheeler and J.K. Thomas, "Photochemistry of the Uranyl Ion in Colloidal Silica Solution", J. Phys. Chem., 88(4), 750-754 (1984).

[12] H. Moll, G. Geipel, V. Brendler, G. Berhard, and H. Nitsche, "Interaction of Uranium(VI) with Silicic Acid in Aqueous Solutions Studied by Time-Resolved Laser-Induced Fluorescence Spectroscopy (TRLFS)", J. Alloys Compd., 271-273, 765-768 (1998).

[13] U. Gabriel, L. Charlet, C.W. Schläpfer, J.C. Vial, A. Brachmann, and G. Geipel, "Uranyl Surface Speciation on Silica Particles Studied by Time-Resolved Laser-Induced Fluorescence Spectroscopy", J. Colloid Interface Sci., 239(2), 358-368 (2001).

[14] C.J. Chisholm-Brause, J.M. Berg, K.M. Little, R.A. Matzner, and D.E. Morris, "Uranyl Sorption by Smectites: Spectroscopic Assessment of Thermodynamic Modelling", J. Colloid Interface Sci., 277, 366-382 (2004).

[15] P. Trepte and V. Brendler, Supporting Information in A. Krepelova, V. Brendler, S. Sachs, N. Baumann, and G. Bernhard, "U(VI)-Kaolinite Surface Complexation in Absence and Presence of Humic Acid Studied by TRLFS", Environ. Sci. Technol., 41(17), 6142-6147 (2007).

[16] G. Othmane, T. Allard, T. Vercouter, G. Morin, M. Fayek, and G. Calas, "Luminescence of Uranium-Bearing Opals: Origin and Use as a pH Record", Chem. Geol., 423, 1-6 (2016).

[17] C.J. Chisholm-Brause, J.M. Berg, R.A. Matzner, and D.E. Morris, "Uranium(VI) Sorption Complexes on Montmorillonite as a Function of Solution Chemistry", J. Colloid Interface Sci., 233(1), 38-49 (2001).

[18] N. Baumann, V. Brendler, T. Arnold, G. Geipel, and G. Bernhard, "Uranyl Sorption Onto Gibbsite Studied by Time-Resolved Laser-Induced Fluorescence Spectroscopy (TRLFS)", J. Colloid Interface Sci., 290(2), 318-324 (2005).

[19] T. Arnold, S. Utsunomiya, G. Geipel, R.C. Ewing, N. Baumann, and V. Brendler, "Adsorbed U(VI) Surface Species on Muscovite Identified by Laser Fluorescence Spectroscopy and Transmission Electron Microscopy", Environ. Sci. Technol., 40(15), 4646-4652 (2006).

[20] Z. Wang, J.M. Zachara, P.L. Gassman, C. Liu, O. Qafoku, W. Yantasee, and J.G. Catalano, "Fluorescence Spectroscopy of U(VI)-Silicates and U(VI)-Contaminated Hanford Sediment", Geochim. Cosmochim. Acta., 69(6), 1391-1403 (2005).

[21] A.S. Saleh, J.Y. Lee, Y. Jo, and J.I. Yun, "Uranium(VI) Sorption Complexes on Silica in the Presence of Calcium and Carbonate", J. Environ. Radioact., 182, 63-69 (2018).

[22] M.J. Comarmond, R. Steudtner, M. Stockmann, K. Heim, K. Müller, V. Brendrer, T.E. Payne, and H. Foerstendorf, "The Sorption Process of U(VI) onto SiO_2 in the Presence of Phosphate: from Binary Surface Species to Precipitation", Environ. Sci. Technol., 50(21), 11610-11618 (2016).

[23] B. Drobot, R. Steudtner, J. Raff, G. Geipel, V. Brendler, and S. Tsushima, "Combination Luminescence Spectroscopy, Parallel Factor Analysis and Quantum Chemistry to Reveal Metal Speciation - A Case Study of Uranyl(VI) Hydrolysis", Chem. Sci., 6(2), 964-972 (2015).

[24] C. Moulin, I. Laszak, V. Moulin, and C. Tondre, "Time-Resolved Laser-Induced Fluorescence as a Unique Tool for Low-Level Uranium Speciation", Appl. Spectrosc., 52(4), 528-535 (1998).

[25] G. Wang, Y. Su, and D.L. Monts, "Parametric Investigation of Laser-Induced Fluorescence of Solid-State Uranyl Compounds", J. Phys. Chem. A., 112(42), 10502-10508 (2008).

[26] E.S. Ilton, Z. Wang, J.F. Boily, O. Qafoku, K.M. Rosso, and S.C. Smith, "The Effect of pH and Time on the Extractability and Speciation of Uranium(VI) Sorbed to SiO_2", Environ. Sci. Technol., 46(12), 6604-6611 (2012).

[27] G. Meinrath, "Uranium(VI) Speciation by Spectroscopy", J. Radioanal. Nucl. Chem., 224(1-2), 119-126 (1997).

[28] J.T. Bell and R.E. Biggers, "The Absorption Spectrum of the Uranyl Ion in Perchlorate Media Part II. *The Effects of Hydrolysis on the Resolved Spectral Bands", J. Mol. Spectrosc., 22(1-4), 262-271 (1967).

[29] J.T. Bell and R.E. Biggers, "Absorption Spectrum of the Uranyl Ion in Perchlorate Media Part III. Resolution of the Ultraviolet Band Structure; Some Conclusions Concerning the Excited State of UO_2^{2+}", J. Mol. Spectrosc., 25(3), 312-329 (1968).

[30] R.G. Denning, "Electronic Structure and Bonding in Actinyl Ions and their Analogs", J. Phys. Chem. A.,

111(20), 4125-4143 (2007).

[31] M.P. Redmond, S.M. Cornet, S.D. Woodall, D. Whittaker, D. Collison, M. Helliwell, and L.S. Natrajan, "Probing the Local Coordination Environment and Nuclearity of Uranyl(VI) Complexes in Non-aqueous Media by Emission Spectroscopy", Dalton Trans., 40(15), 3914-3926 (2011).

[32] P. Harvey, A. Nonat, C. Platas-Iglesias, L.S. Natrajan, and L.J. Charbonnière, "Sensing Uranyl(VI) Ions by Coordination and Energy Transfer to a Luminescent Europium(III) Complex", Angew. Chem. Int. Ed., 130(131), 10069-10072 (2018).

[33] S. Maji, S. Kumar, and S. Kalyanasundaram, "Luminescence Studies of Uranyl-Aliphatic Dicarboxylic Acid Complexes in Acetonitrile Medium", Radichim Acta., 108(5), 361-373 (2020).